SPACE SCIENCES

Gyroresonant wave-particle interactions with chorus waves during extreme depletions of plasma density in the Van Allen radiation belts

Hayley J. Allison[1]*, Yuri Y. Shprits[1,2,3], Irina S. Zhelavskaya[1,2], Dedong Wang[1], Artem G. Smirnov[1,2]

The Van Allen Probes mission provides unique measurements of the most energetic radiation belt electrons at ultrarelativistic energies. Simultaneous observations of plasma waves allow for the routine inference of total plasma number density, a parameter that is very difficult to measure directly. On the basis of long-term observations in 2015, we show that the underlying plasma density has a controlling effect over acceleration to ultrarelativistic energies, which occurs only when the plasma number density drops down to very low values (~10 cm^{-3}). Such low density creates preferential conditions for local diffusive acceleration of electrons from hundreds of kilo–electron volts up to >7 MeV. While previous models could not reproduce the local acceleration of electrons to such high energies, here we complement the observations with a numerical model to show that the conditions of extreme cold plasma depletion result in acceleration up to >7 MeV.

INTRODUCTION

The Van Allen radiation belts are regions of highly energetic particles trapped in the near-Earth space environment by the terrestrial magnetic field. Earth's electron radiation belt region is highly variable, dynamic both in content and in the energy range of trapped electrons. In the past, the radiation belts were believed to behave as a bulk population; however, recent satellite measurements (*1*) have since shown an energy dependence to the particle behavior. In particular, recent observations from the Relativistic Electron Proton Telescope (REPT) on the Van Allen Probes showed that the dynamics of ultrarelativistic electrons may be very different (*2*, *3*) to populations of relativistic ~1-MeV energies. While commonly considered 1-MeV electrons exhibit frequent flux intensifications during geomagnetic storms, enhancements at the ultrarelativistic energy of 7.7 MeV are relatively infrequent, with none observed during the whole of 2014. As these energies have not been accurately measured by previous missions, the understanding of how these particles can be accelerated is incomplete, and various suggestions and speculations have been put forth ever since accurate measurements became available.

Radiation belt electrons can be accelerated through resonant interactions with naturally occurring whistler mode chorus plasma waves (*4*–*6*), which are fluctuations of electric and magnetic field. Energization via chorus wave interactions is one of the key mechanisms responsible for flux enhancements in the core populations of the radiation belts, both at Earth (*7*) and at Jupiter (*8*). Previous studies (*3*, *9*), based on statistical wave and plasma properties, concluded that, generally, local acceleration by chorus waves reduces for >3-MeV electrons, and chorus wave acceleration alone seemed questionable to accelerate electrons to >7 MeV within the observed time scales. Inward radial diffusion offers another explanation for energization; however, to reach >7 MeV, a multi–megaelectron volt source population is required near the last closed drift shell (outer boundary of the radiation belt region). As a result of substorm-induced electric fields, relativistic electrons can occasionally be injected to geostationary orbit (*10*). However, these injections are rare, and in a dipole magnetic field, a seed population of 3.4 MeV is required to explain the enhancement of 7.7 MeV flux at $L = 4$ (assuming 90° particles).

A number of recent studies [e.g., (*11*)] have suggested that the combination of both chorus acceleration and inward radial diffusion, as a two-step process, may explain the occurrence of ultrarelativistic enhancements, with local chorus acceleration providing the source population on which radial diffusion acts. However, analysis of phase space density profiles for two consecutive geomagnetic storms in October 2012 indicated that local acceleration energized electrons directly to ultrarelativistic energies (*12*). How local acceleration was able to reach such high energies and the conditions that allow for such acceleration are, thus far, unclear. In this study, we show that extreme depletions of plasma density, observed by Van Allen Probes, create unique conditions for local acceleration by chorus waves to multi–megaelectron volt energies, producing >7-MeV flux enhancements.

RESULTS

Electron density variations in the plasma trough

Chorus waves propagate outside a high-density bubble of plasma, corotating with Earth, known as the plasmasphere. For the region outside the plasmasphere, called the plasma trough, several statistical electron density models have been developed (*13*–*15*). In this study, electron density values, n_e, were obtained from the Van Allen Probe A Electric and Magnetic Field Instrument Suite and Integrated Science (EMFISIS) data (*16*) with the Neural-network-based Upper hybrid Resonance Determination (NURD) algorithm (*17*). The density throughout 2015, both inside and outside the plasmasphere, is shown in Fig. 1C, and a highly variable plasmapause location is evident. Nine 7.7-MeV enhancement events were identified (magenta lines in Fig. 1) during 2015, occurring far less frequently than flux enhancements at 1.8 MeV (Fig. 1A). While the L^* (approximately radial distance

[1]GFZ German Centre for Geosciences, Potsdam, Germany. [2]Institute of Physics and Astronomy, University of Potsdam, Potsdam, Germany. [3]Department of Earth, Planetary, and Space Science, University of California, Los Angeles, Los Angeles, CA, USA.
*Corresponding author. Email: haylis@gfz-potsdam.de

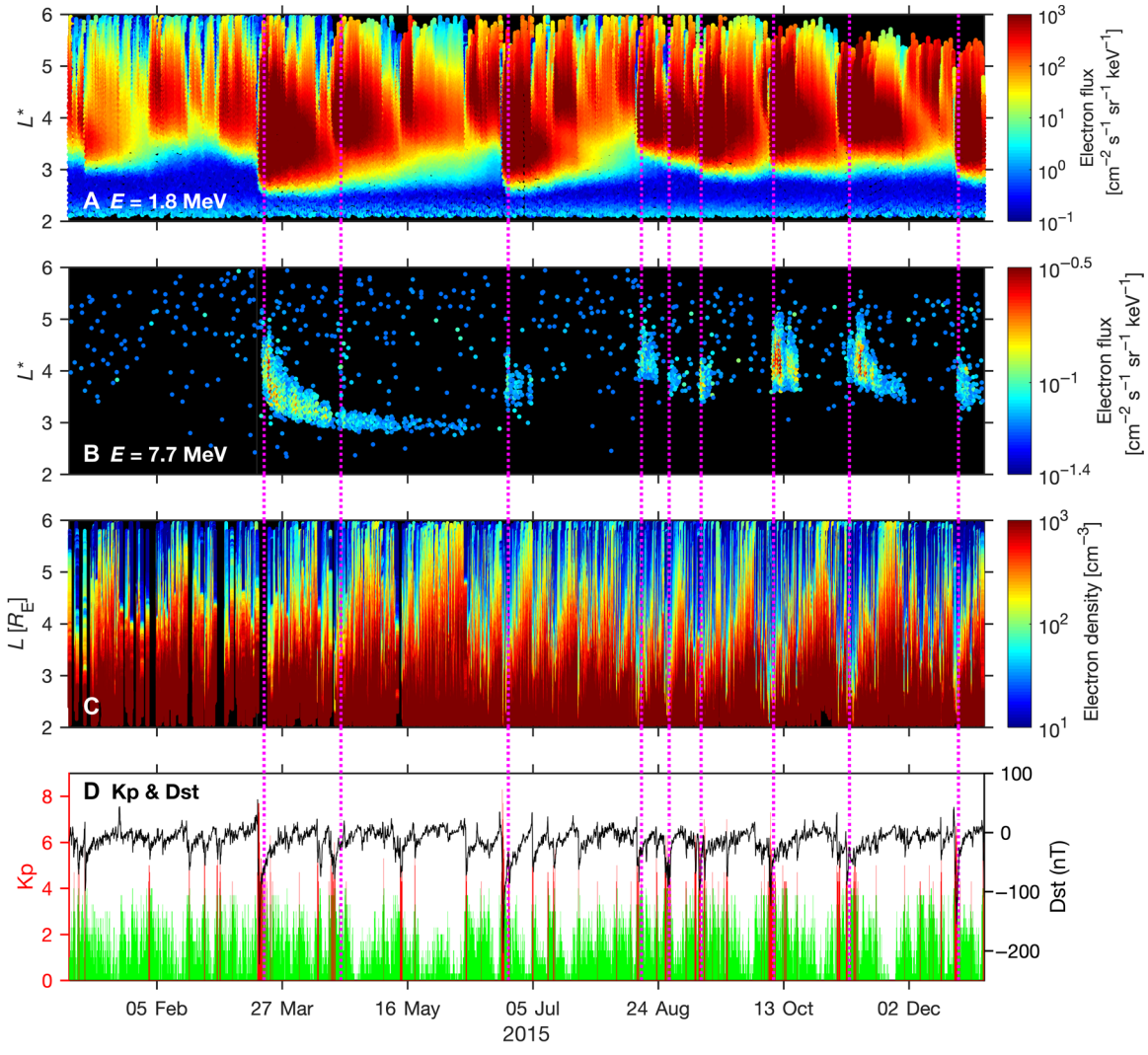

Fig. 1. An overview of the electron flux, density, and geomagnetic activity throughout 2015. The electron flux is shown at 1.8 MeV, 90° local pitch angle (**A**) and at 7.7 MeV, 90° local pitch angle (**B**) as measured by REPT on Van Allen Probe A. In both panels, only measurements above the background threshold of the instrument are shown. Electron density data obtained using the NURD algorithm are also presented (**C**). Last, the Kp (semilogarithmic scale showing the geomagnetic field disturbance) and Dst (disturbance storm time index; a measure of the geomagnetic storm intensity) index are shown in (**D**) for reference. Kp values greater than 4 are highlighted as red bars. Magenta dotted lines mark the 7.7-MeV enhancement event periods. Comparison of the density evolution with the observations of ultrarelativistic electrons shows that enhancements occur only when density is depleted.

in the equatorial plane, calculated for magnetic coordinates) extent of the 7.7-MeV flux enhancement varies between each of the events, all nine penetrate inside $L^* = 4$ and are observed in the heart of the outer radiation belt zone. Geostationary Operational Environmental Satellite (GOES) data for each of the nine events are shown in fig. S1.

The geometric mean of the trough electron densities in 0.1-L bins shows values comparable to two trough density models: the Sheeley *et al.* (*13*) model (orange line) and the Denton *et al.* (*14*) model (blue line, Fig. 2A). The SD of the logged electron densities is given as error bars in Fig. 2A, and the two density models are within the SD range for all L values. The L values shown are limited to $L \geq 3$, as the Sheeley *et al.* (*13*) model is only valid for $3 \leq L \leq 7$. Above $L = 6$, there are fewer NURD density measurements as a result of the Van Allen Probes' orbit. Figure 2A demonstrates that the average electron densities from NURD generally agree with the results of previous studies (*13*, *14*, *17*).

Figure 2B shows the NURD electron plasma density at $L = 4$, throughout 2015, as black points. Only density values outside the plasmasphere are considered. Trough region density values given by the Denton *et al.* (*14*) model (blue) and the Sheeley *et al.* (*13*) model (orange) are also plotted for comparison. For the Sheeley *et al.* (*13*) model, the magnetic local time (MLT) of the Van Allen Probe A was used for the calculation as the probe's orbit precesses throughout the year (see mini plots at the top of Fig. 2B). The vertical magenta lines are as shown in Fig. 1 and mark the 7.7-MeV enhancement times.

While, on average, the density is comparable to the two statistical models, there are periods when the actual density falls below the average values by up to an order of magnitude. During each 7.7-MeV enhancement event, the density is consistently lower than the

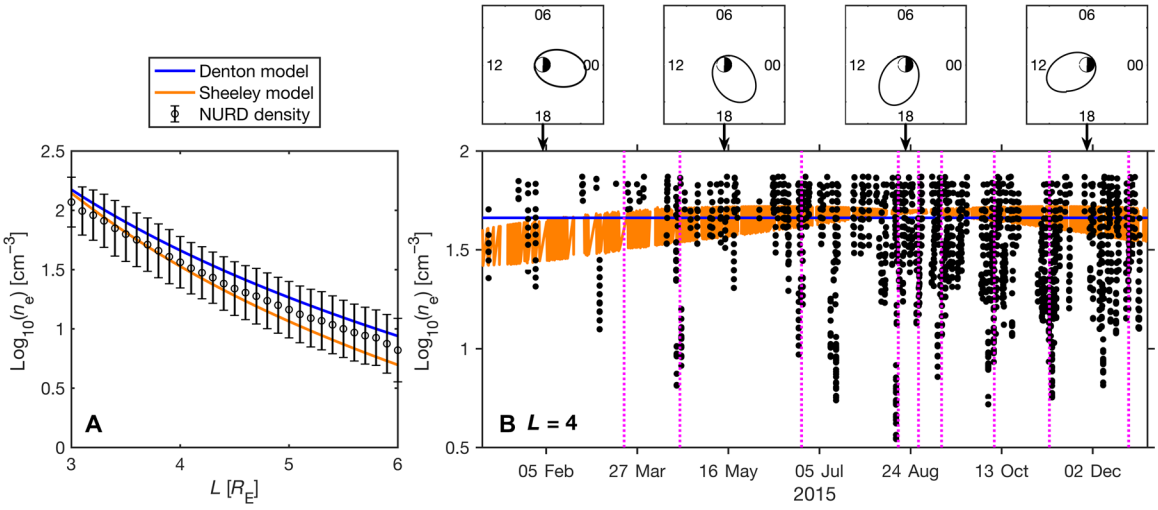

Fig. 2. A comparison of NURD-determined electron density values (black points) outside the plasmasphere to the trough density model of Denton *et al.* (*14*) (blue line) and Sheeley *et al.* (*13*) (orange line). The mean of the log (n_e) NURD data is shown (**A**) for $3 \leq L \leq 6$ in 0.1-L increments with the SD given as error bars (black points). The Denton *et al.* (*14*) and Sheeley *et al.* (*13*) models are included as blue and orange lines, respectively, where the Sheeley *et al.* (*13*) model was calculated at MLT = 0 for this comparison. The time evolution of the NURD density values (black points) outside the plasmasphere at $L = 4$ is shown throughout 2015 (**B**). The trough density models of Denton *et al.* (*14*) (blue line) and Sheeley *et al.* (*13*) (orange line) are included for reference. Mini plots show the MLT coverage of the Van Allen Probe A orbit at four times throughout the year, and magenta vertical lines indicate the 7.7-MeV enhancement times. Increases in the ultrarelativistic electrons coincide with these density depletions.

two considered standard density models, representing average densities. Note that, for the first 7.7-MeV event in March, NURD did not return any quality flags equal to 1 (highest data quality level that we exclusively used here), yielding a data gap. However, examination of Fig. 1C shows that the plasmasphere is eroded immediately following the data gap, suggesting that the density was likely also low during this event. The differences between the density and the models during the enhancements can be greater than a factor of 10 but are generally a factor of ~6 (Fig. 2B). Although Fig. 2B considers variations at $L = 4$ exclusively, the electron plasma density surrounding the times marked by the magenta lines in Fig. 1 indicates that the density is typically reduced for L outside the plasmapause over multiple orbits of the probe. As different MLT values are sampled during the inbound and outbound parts of the orbit, we suggest that the density decrease is not localized in MLT but representative of a global reduction throughout the trough region.

Density values lower than the statistical models are also observed outside of the 7.7-MeV enhancement times; however, considering Fig. 1E, these tend to occur during periods of low Kp, indicating times when chorus wave activity (*18*) may be low and acceleration is inhibited because of the lack of wave activity.

Figure 3 shows an example of one of the 7.7-MeV enhancement events from the time period shown in Fig. 1. Before the geomagnetic storm [Dst (disturbance storm time index) minimum of −124 nT], which occurred at the start of October 2015 (minimum Dst time at October 7, 22:00), a sustained population of 7.7-MeV electrons was not present in the outer radiation belt. The 7.7-MeV flux then increased to above the background threshold of the REPT energy channel a little over a day after the 1.8-MeV flux was enhanced to above prestorm levels. Before the 7.7-MeV enhancement, the Kp index indicated active geomagnetic conditions, with a maximum Kp of 7.3. During the event, Van Allen Probe A primarily sampled the postnoon MLT sector and is therefore not optimally located to measure chorus wave activity, particularly upper band chorus (*19*). Nevertheless, the square of the wave magnetic amplitudes, B_w^2, shows that chorus waves were active during this period (Fig. 3D). In fig. S2, the Wang *et al.* (*19*) empirical chorus wave model is compared with these chorus observations. Even for the postnoon sector, the NURD electron plasma density indicates a greatly eroded plasmasphere and low plasma density in the trough region at $L = 4$ in the days preceding the first increase in the 7.7-MeV flux.

Effect of changing density on the diffusion coefficients

Changes in the electron density affect the electron plasma frequency, f_{pe}, which is a fundamental quantity, showing the frequency of electrostatic fluctuations in a cold plasma. As plasma is a dispersive medium, changes in f_{pe}, in turn, alter the phase speed and wave number corresponding to each frequency. Chorus waves resonantly interact with electrons at frequencies and wave numbers corresponding to intersections between the dispersion relation and the cyclotron resonance condition. The changes in f_{pe} alter the electron energies and pitch angles, α, at which resonant interactions with chorus waves occur (*5*, *7*), where pitch angle is defined as the angle between the particle's velocity vector and the background magnetic field.

Chorus emissions are typically quasi-coherent discrete elements with frequency chirping originating from nonlinear effects during the generation process. Chorus waveforms often show quasi-periodic modulations of amplitude, leading to a subpacket structure (*20*). Despite being inherently a nonlinear phenomenon, quasi-linear simulations are often successful in reproducing the observed effects of chorus wave-particle interactions [e.g., (*21*)], when individual waves are not large enough to induce nonlinear particle behavior such as phase trapping and nonlinear scattering (*22*, *23*). Other work has recently shown that, even for intense chorus waves, a quasi-linear approach can be a good approximation, as phase decoherence can mitigate nonlinear effects (*24*).

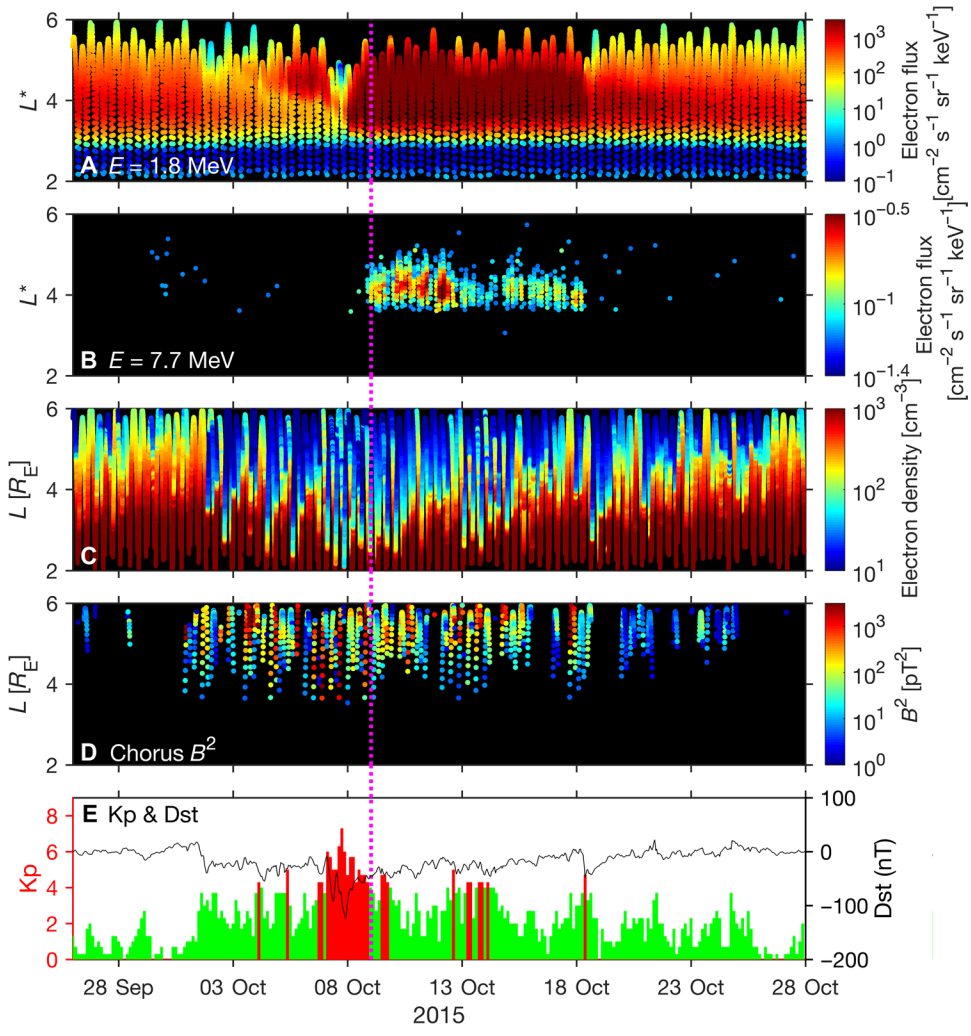

Fig. 3. An example of one of the 7.7-MeV enhancement events seen in Fig. 1. The electron flux from the REPT instrument of Van Allen Probe A is shown at 1.8 MeV, 90° local pitch angle (**A**) and at 7.7 MeV, 90° local pitch angle (**B**). As for Fig. 1, in both panels, only measurements above the background threshold of the instrument are shown. Electron density data obtained using the NURD algorithm are also presented for the example event (**C**). The square of wave magnetic amplitudes sampled by the EMFISIS wave form receiver (level 2 data) (*16*), B^2, are integrated over the lower band (**D**) chorus frequency range given by Wang *et al.* (*19*). The spacecraft primarily samples the postnoon MLT sector during this period and is therefore not well situated to measure upper band chorus activity (*19*). The chorus B^2 data are time averaged over 10-min intervals. The Kp and Dst indices are shown in (**E**). Kp values greater than 4 are highlighted as red bars. A magenta line marks the identified 7.7-MeV enhancement time.

Quasi-linear theory (*25*–*27*) describes local acceleration as diffusion in momentum space, from low energy to high energy. The evolution of Earth's electron radiation belt can therefore be described by a diffusion equation, with diffusion coefficients that incorporate the effect of wave-particle interactions. Diffusion parameters depend on many variables, such as the wave characteristics. To isolate the effects of n_e on the diffusion coefficients, we use realistic statistical results for the wave characteristics (see the "Calculation of diffusion coefficients" section) and then calculate D_{pp} for the values of n_e considered here. Figure 4A shows the energy diffusion coefficients from lower band chorus in units of days (logarithmic color scale), calculated using the Sheeley *et al.* (*13*) density model, at $L = 4$. In Fig. 4B, the energy diffusion coefficients have been calculated with a density of 10 cm^{-3}, a value selected by considering the NURD density data during the 7.7-MeV events in Fig. 2A. Other than the density, all parameters are identical between Fig. 4A and Fig. 4B. The reduction in density results in an increase in the energy diffusion coefficients across all energies, in agreement with previous work (*21*). D_{pp} (the momentum diffusion coefficient related to energy diffusion) has increased notably at energies >1 MeV and pitch angles >40° between Fig. 4A and Fig. 4B. For example, let us consider D_{pp} at ~6 MeV, 70°, where the increase is approximately a factor of 10. The D_{pp} increase across all energies following the reduction in density is consistent with the observations presented in Fig. 1, where the 1.8-MeV flux accompanying the 7.7-MeV enhancements tends to be the highest throughout the year, routinely exceeding 10^3 cm^{-2} s^{-1} sr^{-1} keV^{-1} at $L^* = 4$. Comparing Fig. 4 (C and D) shows that the reduction in density also results in enhanced energy diffusion from upper band chorus; however, changes are less pronounced than for the lower band and primarily affect <1-MeV energies.

The $D_{\alpha\alpha}$ and $D_{\alpha p}$ diffusion coefficients for pitch angle diffusion and mixed momentum pitch angle diffusion are also affected by the changing density (see figs. S3 and S4). Electrons that, at the magnetic equator, have near 0° pitch angles will collide with the atmosphere

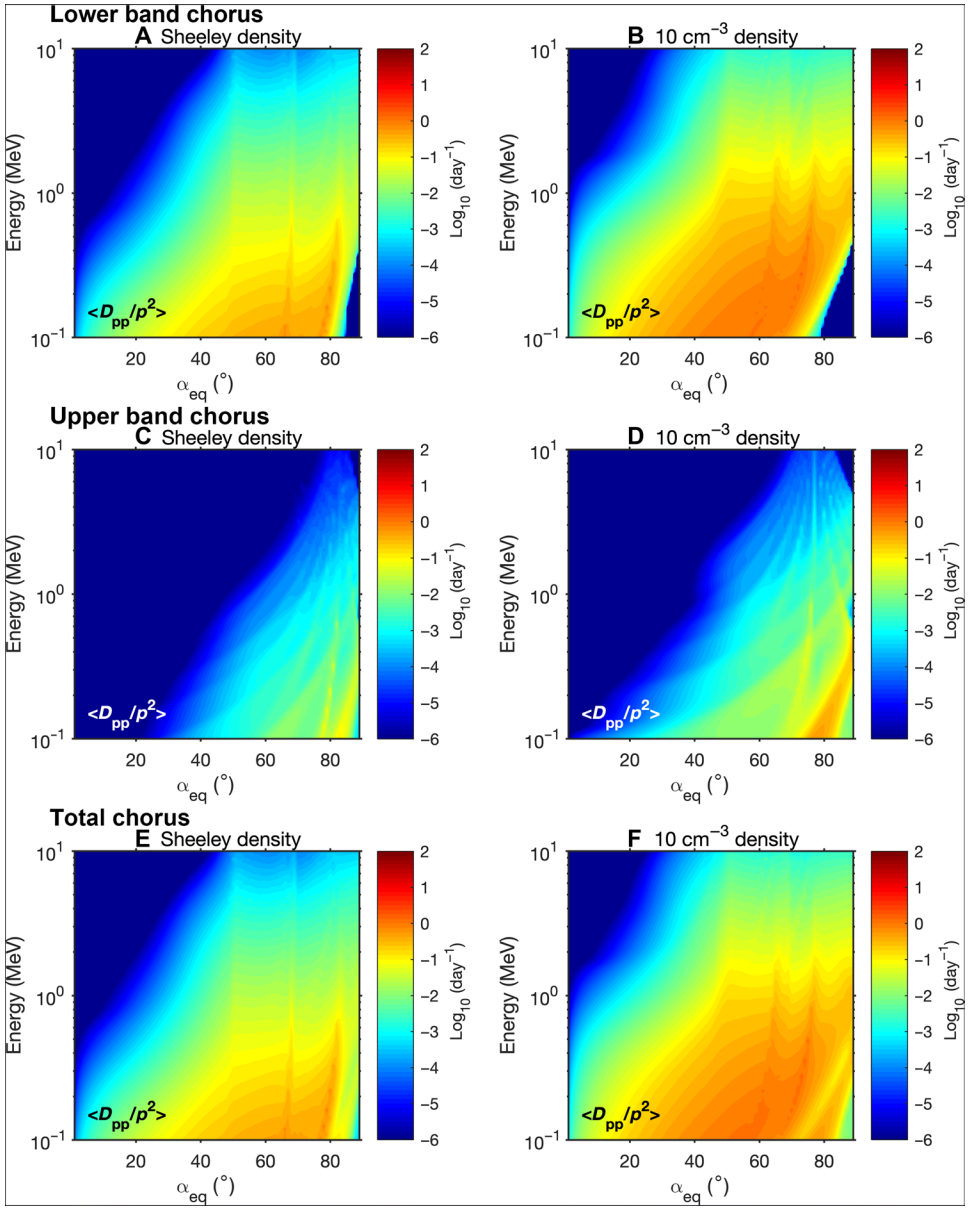

Fig. 4. Drift- and bounce-averaged energy diffusion coefficients, D_{pp}, at $L = 4$ in units of $\log_{10}(\text{day}^{-1})$ as a function of energy and equatorial pitch angle. (**A**, **C**, and **E**) Energy diffusion coefficients calculated using the Sheeley density model (which corresponds to a density of 33.7 cm^{-3} at MLT = 0 and 44.8 cm^{-3} at MLT = 12) for lower band, upper band, and upper and lower band chorus, respectively. Likewise, (**B**), (**D**), and (**F**) show the diffusion coefficients for lower band, upper band, and both lower and upper band chorus, calculated assuming a reduced density of 10 cm^{-3}. The D_{pp} coefficients are higher across all energies when the density is reduced.

and are lost from the radiation belts. As a result, pitch angle diffusion, shifting electrons from high to low equatorial pitch angles, results in a loss of particles. Both local acceleration and local loss are enhanced when density is low, and radiation belt dynamics are a delicate balance between acceleration and loss processes. The overall effect of the density-induced changes in the chorus diffusion coefficients on radiation belt populations is explored with a diffusion model in the following section.

Energization to ultrarelativistic energies

The diffusion coefficients are used in the two-dimensional (2D) version (dimensions of pitch angle and momentum) of the Versatile Electron Radiation Belt code [VERB-2D (*28*)] to explore the effect periods of reduced density have on the evolution of the electron population. The following calculations are performed at $L^* = 4$, in the heart of the outer radiation belt.

The initial condition was chosen to be a straight line (in log-log space) from the flux at 100 keV to the flux at 10 MeV, with a simple $f(\alpha) = f(90^\circ)\sin\alpha$ pitch angle distribution assumed for all energies (see the "VERB-2D model runs" section for further details). VERB-2D was run from this initial condition, first with the diffusion coefficients calculated using the Sheeley *et al.* (*13*) density model (Fig. 5, A and B) and then again with the diffusion coefficients calculated with the 10-cm^{-3} density (Fig. 5, C and D). Figure 5 shows

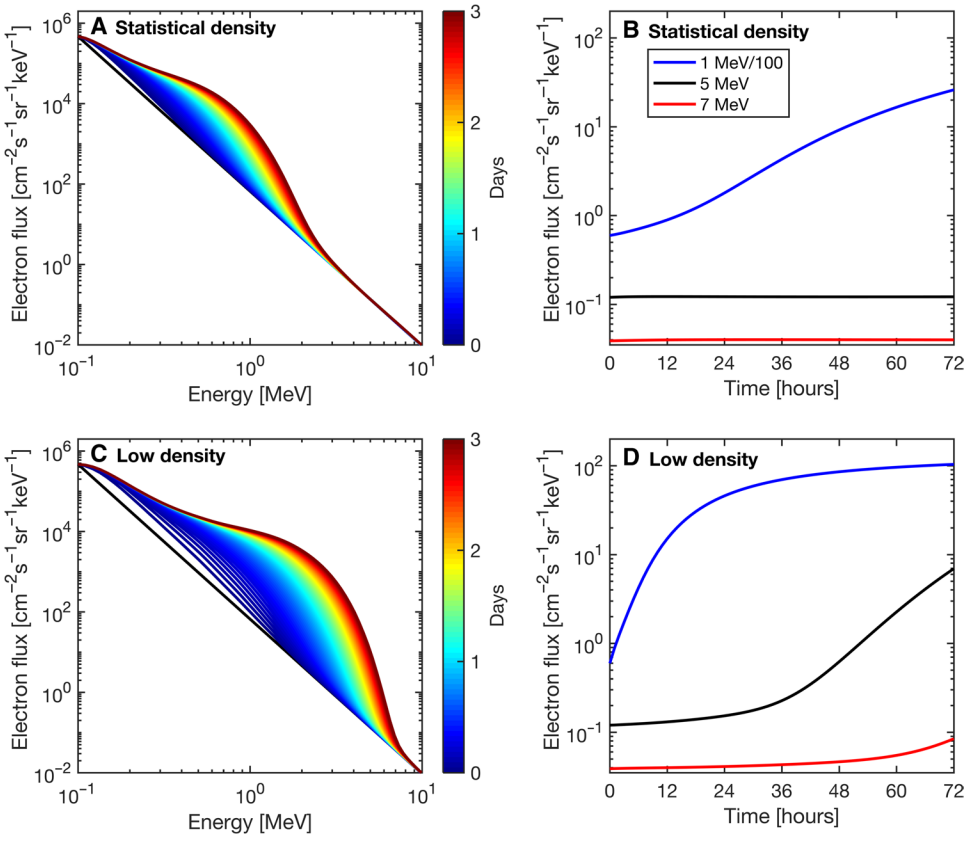

Fig. 5. VERB-2D simulations of the evolution of the electron flux at $L^* = 4$, $\alpha = 70°$ over a 3-day period. The calculation includes pitch angle and energy diffusion, including the cross terms. (**A** and **B**) A model run, including upper and lower band chorus waves, with diffusion coefficients calculated using the Sheeley statistical density model (which corresponds to a density of 33.7 cm^{-3} at MLT = 0 and 44.8 cm^{-3} at MLT = 12). (A) Evolution of the electron energy distribution, in 1-hour intervals, where the line color indicates the model time lapsed in days. (B) shows how the electron flux corresponding to 1-, 5-, and 7-MeV changes with time. Note that the 1-MeV flux is divided by a factor of 100. (**C**) and (**D**) take the same form as (A) and (B) but instead use the diffusion coefficients calculated with the reduced density of 10 cm^{-3}. Simulations show that in the depleted density environment chorus efficiently accelerates electrons from hundreds of kilo–electron volt to multi–megaelectron volt energies.

the evolving energy spectrum for 70° electrons in intervals of 1 hour. The phase space density dynamics over a 3-day period were simulated. Justifications for why we use a 3-day simulation time are given in the discussion surrounding fig. S5. In fig. S6, we consider the output of VERB-2D using chorus diffusion coefficients calculated from one further density value, a density of 25 cm^{-3}. We selected this density as an intermediate value between the Sheeley *et al.* (*13*) model and 10 cm^{-3}.

A comparison of Fig. 5 (A and C) demonstrates that the reduction in density allows for higher energy populations to be enhanced by chorus-induced energy diffusion. With density values given by a statistical model, (*13*), the flux displays an enhancement up to ~3 MeV, consistent with previous results (*3*, *7*), and at higher energies, no change is observed from the initial condition within the 3 days. When the density is reduced, we observe a faster enhancement at the relativistic energy of 1 MeV (Fig. 5D) over a 12-hour time scale. Furthermore, the upper energy threshold of the enhancement is increased, and the flux is enhanced for $\lesssim$8 MeV. Figure S7 shows the influence of the upper and lower band chorus waves on the flux evolution separately for the two density regimes.

The Van Allen Probe observations in Fig. 3 indicate that for the October 2015 event, there is a ~1-day delay between the 1.8-MeV electron flux first exceeding 10^3 cm^{-2} s^{-1} sr^{-1} keV^{-1} and the 7.7-MeV flux being enhanced. Consistent with the observations, the VERB-2D model run shown in Fig. 5C also exhibits a time delay between the enhancements of these populations. The model results indicate the time difference between the 1.8-MeV flux reaching 10^3 cm^{-2} s^{-1} sr^{-1} keV^{-1} and the >7-MeV flux increasing above the initial level is ~1.5 days. Note that we have used a general initial condition for the VERB-2D model run and also assume a constant chorus wave power equal to Kp = 4. The Kp index before the 7.7-MeV enhancement was higher than Kp = 4 in the October 2015 event, with a maximum of Kp = 7.3.

DISCUSSION

The results presented in the previous section demonstrate that during periods when the trough density is significantly depleted below average levels, chorus waves, if present, are capable of producing local enhancements of >7-MeV electrons. We have isolated the effects of local acceleration from those of radial diffusion by using the 2D version of the VERB model and, in doing so, demonstrate that these energies may be reached locally, without involving radial transport. However, radial diffusion is also an active process in the radiation belt region. By gradually moving electrons into regions of stronger magnetic field, the particle energy is increased by betatron and Fermi acceleration (*29*). In this regard, inward radial diffusion may also

increase enhancements at ultrarelativistic energies via two-step acceleration or contribute to the hardening of the phase space density spectrum, resulting in faster energy diffusion (*30*). Depending on the radial gradients in phase space density, radial diffusion may also transport locally accelerated electrons outward, toward the geostationary orbit.

While in this work we have focused on the extreme case of energization to 7.7 MeV, Fig. 5D also shows that, when the density is reduced, chorus waves accelerate electrons to >1 MeV on shorter time scales, which is consistent with previous studies (*21*, *31*, *32*). In Fig. 5D, the 1-MeV flux has increased in a 1-hour interval (lines are shown in 1-hour increments, and at 1 MeV, a distinct increase can be observed between the initial condition shown by the black line and the subsequent line). This was not the case for the statistical (*13*) density model (Fig. 5A), where the same increase took more than 12 hours. Therefore reductions in density may also account for rapid >1-MeV flux enhancements observed, particularly following flux dropout events.

Density values in the plasma sheet are of the order of 10^{-1} cm^{-3} (*33*); however, statistically, densities in the trough region tend to be several $\sim 10^{1}$ cm^{-3} (*13*, *14*). This difference may potentially be because plasma can take some time to be lost from the trough, as well as some potential leakage from the plasmasphere. The observations shown in this paper demonstrate that the trough density can drop to near plasmasheet levels, and the resulting conditions lead to efficient energy diffusion by whistler mode chorus waves, allowing acceleration from hundreds of kilo–electron volts to multi-megaelectron volt energies. Such extreme density drops are rather infrequent, occurring only a handful of times during 2015. A preliminary analysis (fig. S8) shows that the density drops coincide with times of prolonged convective activity. However, further work is required on the causes and circumstances that allow the density to reduce to lower-than-average levels. In addition, the Van Allen Probes primarily measure close to the magnetic equator, and new datasets are required to explore potential latitudinal dependencies in the density reduction.

The 7.7-MeV electron flux throughout 2015 (Fig. 1B) shows variability between the enhancement events, both in flux level and in the L^* extent. The radiation belt response to local acceleration is likely to depend on the characteristics and occurrence of chorus waves, as well as on how long and over what spatial scale waves are present and n_e is depressed. In this study, a statistical chorus wave model is used when calculating diffusion coefficients to isolate the effects of the density variations. Further work will consider the strength and duration of measured chorus wave activity during different ultrarelativistic enhancement events, alongside the changes in electron density, to better understand the observed variability in the 7.7-MeV flux.

By considering the electron density data from Van Allen Probe A for 2015, we find that the radiation belts extend to ultrarelativistic energies only during times when the density drops significantly below the average values. The reduction in density results in increased lower and upper band chorus-induced energy diffusion, particularly at >3-MeV energies. By using these diffusion coefficients in VERB-2D, we demonstrated that, during the times of low density, the electrons can be accelerated by whistler mode chorus waves to >7 MeV within 3 days. Whereas when the density was instead given by the Sheeley *et al.* (*13*) model, flux enhancements were limited to <3-MeV energies during the 3-day window. The reduction in electron density also increases the acceleration rate of relativistic ($\gtrsim$1 MeV) electrons in the radiation belt region, with the ~1-MeV population showing an increase in a matter of hours. The results presented here have important implications for understanding the origin of ultrarelativistic electrons in Earth's radiation belts and have potential application to Jupiter, Saturn, and other magnetized plasmas in the Solar System.

MATERIALS AND METHODS

Statistical density models and Van Allen Probe density data

The Sheeley *et al.* (*13*) model used 8 months of data from the sweep frequency receiver onboard the Combined Release and Radiation Effects Satellite (CRRES) to identify the upper hybrid resonance (UHR) frequency. The UHR is a combination of the ion cyclotron frequency and the plasma frequency and can be used to determine the electron density. Sheeley *et al.* (*13*) separated plasmasphere and trough measurements by using a density cutoff and developed a statistical model for both, with the trough density model dependent on MLT and L. An alternative model was developed by Denton *et al.* (*14*) using densities derived from UHR measurements from the Polar Plasma Wave Instrument on the Polar spacecraft. The resulting plasmatrough density model depends only on L and is valid for $L <$ 6.4. Last, the Carpenter and Anderson (*15*) model was constructed from International Sun-Earth Explorer 1 (ISEE 1) sweep frequency receiver observations and whistler observations, where the density profiles were examined by eye to determine whether the measurements lay inside or outside the plasmasphere. Their model is valid over a limited range of MLT and for $2.25 \leq L \leq 8$. Owing to the limited MLT range, we have not considered the Carpenter and Anderson (*15*) model in this study.

The three statistical models for the plasma trough density are activity independent. Because of limited observations, Carpenter and Anderson (*15*) did not consider changes in geomagnetic activity. On the other hand, Sheeley *et al.* (*13*) included geomagnetic activity in the form of Kp_{max} (the maximum value of Kp in the previous 24 hours) but found the trough density to be independent of this variable. Denton *et al.* (*14*) also took account of activity (in the form of a weighted average of Kp over 3 days) but were unable to firmly conclude whether an activity dependence was present in the data. As a result, an activity variation was not included in either model. The Sheeley *et al.* (*13*) and Denton *et al.* (*14*) density models are frequently used when calculating chorus diffusion coefficients (*34*–*36*), and therefore, these diffusion coefficients also do not contain any activity-dependent changes in the electron density.

The NURD density data used in this study are provided with an accompanying quality flag that indicates the confidence in the UHR frequency retrieval. Only measurements corresponding to quality flag 1, signifying the highest quality data, have been used for the analysis. Measurements taken outside the plasmasphere were isolated using the cutoff threshold given by Sheeley *et al.* (*13*)

$$n_{\text{threshold}} = (10\ \text{cm}^{-3})(6.6/L)^4 \quad (1)$$

Electron plasma density measurements can be challenging to determine as the UHR is not always apparent in spectograms. Electron cyclotron harmonic waves are electrostatic waves that occur near the UHR during active periods and can result in the UHR being over- or underestimated (*17*), therefore returning density values that are not as representative of the current state of the system. Here, we have attempted to mitigate this by only using NURD data marked

as "good data" (quality flag 1). As a result, lower density values than the ones shown in Fig. 2 may occur and therefore further change how the waves in the magnetosphere interact with trapped electron populations. In addition, for the investigation period, Van Allen Probe A sampled the dusk side of Earth (see mini plots Fig. 2A). At least in a statistical sense, the dusk side electron plasma density tends to be higher than on the dawn side (*9*, *13*), and so, dawn side densities may be lower than the values shown in Fig. 2.

Identifying 7.7-MeV enhancement events

For both the 1.8- and 7.7-MeV REPT measurements shown in Figs. 1 and 3, flux values at or below the background threshold for the respective energy channel (*37*) have been removed from the dataset. The 7.7-MeV enhancement times are defined to be when the 7.7-MeV flux exceeded the background threshold at $L^* = 4$ (within ±0.1 L^*) for two or more consecutive passes. The first pass was then used as the enhancement time. We considered the flux at $L^* = 4$, as all the 7.7-MeV enhancements during 2015 extended to this L^*. To identify a new enhancement, the 7.7-MeV flux must first drop down to below background at $L^* = 4$.

Calculation of diffusion coefficients

In this work, we use the common assumption that the chorus wave field exhibits a spread in both frequency and wave normal angle. Electrons resonate with the waves according to the resonance condition. We therefore locally determine the particle energies and pitch angle range for which both the resonance condition and cold plasma dispersion relation are satisfied. Resonant interactions can continue until the waves are no longer present or until no part of the particle distribution is in resonance with the wave frequencies between the upper and lower frequency cutoffs. The width of the wave frequency range can be broadened by the width of the wave normal angle distribution in latitude.

Quasi-linear theory describes the mean effect of these resonant wave-particle interactions on the electron phase space density distribution as a diffusion problem (*27*). As long as there are waves active, particles with energies and pitch angles in resonance with the waves between the upper and lower frequency cutoffs, and gradients in phase space density, then a series of resonant interactions will act to remove the phase space density gradients via both pitch angle and energy scattering. Associated diffusion coefficients describe the rate of diffusion over momentum and pitch angle space.

We use the Full Diffusion Code [FDC; (*38*–*40*)] to calculate the bounce- and drift-averaged chorus diffusion coefficients for two different electron densities. FDC solves the cold plasma dispersion relation alongside the resonance condition and returns fully relativistic, quasi-linear D_{pp}, $D_{\alpha\alpha}$, and $D_{p\alpha}$ coefficients for resonant wave-particle interactions in a magnetized plasma.

In accordance with previous work (*9*, *34*, *41*), we have considered harmonic resonances from −5 to 5, including the $n = 0$ Landau resonance. The diffusion coefficients are averaged over an electron's bounce path between the particle's magnetic mirror points, incorporating the latitudinal variation of the chorus waves. Diffusion coefficients are calculated separately for the day and night MLT sectors and averaged to produce the drift-averaged coefficients. A Gaussian wave normal angle distribution and a polynomial function frequency distribution are assumed, with parameters given by statistical wave models (*19*, *42*, *43*). The frequency distributions of both the upper and lower band chorus waves were taken from a recent study by Wang *et al.* (*19*), where five years of Van Allen Probe A data were used to provide average power spectral density distribution functions for both day side and night side chorus waves, at magnetic latitudes of $\lambda < 10°$ and $10° \leq \lambda < 20°$ [see Figure 14 of the Wang *et al.* (*19*) paper]. On the night side, the lower band chorus wave amplitudes tended toward 0 pT for $\lambda \geq 20°$, while on the day side, there are observations of chorus waves at latitudes higher than 20° (*19*, *34*); however, we do not consider these here. For upper band chorus, observations show large reductions in wave power with increasing distance from the magnetic equator. As a result, we restricted upper band chorus waves to $\lambda < 10°$ and used the appropriate power spectra given by Wang *et al.* (*19*). Latitude-dependent wave normal angle distributions for upper and lower band chorus from Ni *et al.* (*42*) are used, and the chorus wave power is taken from the Kp-parameterized model by Zhu *et al.* (*43*), with Kp = 4 to represent active conditions. With regard to the density, we assume that the density of 10 cm^{-3} applies over all MLT, while with the Sheeley *et al.* (*13*) density model, we use the density at MLT = 12 for the day side and MLT = 0 for the night side. D_{pp}, $D_{\alpha\alpha}$, and $D_{p\alpha}$ coefficients were calculated on the same α and energy grid used in the VERB-2D code (described below).

VERB-2D model runs

All simulations of the electron phase space density were performed using the VERB-2D code (*28*). VERB-2D solves the Fokker-Planck equation for the evolution of the phase space density, f, in coordinates of relativistic momentum, p, and pitch angle, α

$$\frac{\partial f}{\partial t} = \frac{1}{p^2}\frac{\partial}{\partial p}\Big|_{\alpha} p^2\left(D_{pp}\frac{\partial}{\partial p}\Big|_{\alpha} f + D_{p\alpha}\frac{\partial}{\partial \alpha}\Big|_{p} f\right) + \frac{1}{T(\alpha)\sin(2\alpha)}\frac{\partial}{\partial \alpha}\Big|_{p} T(\alpha)\sin(2\alpha)\left(D_{\alpha\alpha}\frac{\partial}{\partial \alpha}\Big|_{p} f + D_{p\alpha}\frac{\partial}{\partial p}\Big|_{\alpha} f\right) - \frac{f}{\tau} \quad (2)$$

The drift- and bounce-averaged diffusion coefficients, D_{pp}, $D_{\alpha\alpha}$, and $D_{p\alpha}$ are shown in Fig. 4 and figs. S3 and S4, respectively. $T(\alpha)$ is a function related to the bounce motion and, in a dipolar magnetic field, can be approximated as

$$T(\alpha) = 1.3802 - 0.3198(\sin\alpha + \sin^2\alpha) \quad (3)$$

The final term of Eq. 2 accounts for atmospheric loss due to Coulomb collisions in the loss cone. The parameter τ is the electron lifetime, taken to be a quarter of the bounce time inside the loss cone and infinite outside. In the calculation, we use a time step of an hour and a grid resolution of 106 × 89 in p and α, respectively.

Four boundary conditions are required to define the calculation domain, at the maximum and minimum values of both p and α. Relativistic momentum, p, is related to the kinetic energy by $E = \sqrt{p^2c^2 + m^2c^4} - mc^2$, and we define $f = 5 \times 10^5$ cm^{-2} s^{-1} sr^{-1} keV^{-1} at the low energy boundary of 100 keV and assume a very low flux of $f = 1.4 \times 10^{-6}$ cm^{-2} s^{-1} sr^{-1} keV^{-1} at the high energy boundary at 100 MeV [chosen so that in the initial condition described below, the flux at 10 MeV is ten times lower than the background threshold of the 10-MeV REPT channel (*37*)]. At the minimum equatorial pitch angle boundary, we use $f = 0$, while at the maximum equatorial pitch angle (89°), the gradient of f in pitch angle is set to zero.

As an initial phase space density distribution, a simple straight line in log-log space is used running from 5×10^5 cm^{-2} s^{-1} sr^{-1} keV^{-1} at the low energy boundary of 100 keV, α = 90°, to 1.4 × 10^{-6} cm^{-2} s^{-1} sr^{-1} keV^{-1} at the high energy boundary at 100 MeV, α = 90°. The initial condition therefore follows the equation $\log_{10}(f(E)) = 1.8493 - (3.8497)\log_{10}(E)$. A simple $f(\alpha) = f(90^{\circ})\sin\alpha$ pitch angle distribution was initially assumed for all energies. The response of the radiation belt is dependent on the preexisting phase space density; however, as we do not attempt to recreate a specific event, we choose a simple form for the initial condition that can be easily reproduced. As discussed above, for the diffusion coefficients used, the chorus wave intensity was set using Kp = 4 and held constant for the 3 days of the simulation. A time-varying wave intensity is more physically representative of chorus waves in the radiation belt region, but this approach is left to later studies.

SUPPLEMENTARY MATERIALS

Supplementary material for this article is available at http://advances.sciencemag.org/cgi/content/full/7/5/eabc0380/DC1

REFERENCES AND NOTES

1. G. D. Reeves, R. H. W. Friedel, B. A. Larsen, R. M. Skoug, H. O. Funsten, S. G. Claudepierre, J. F. Fennell, D. L. Turner, M. H. Denton, H. E. Spence, J. Bernard Blake, D. N. Baker, Energy-dependent dynamics of keV to MeV electrons in the inner zone, outer zone, and slot regions. *J. Geophys. Res. Space Physics* **121**, 397–412 (2016).
2. D. N. Baker, V. Hoxie, H. Zhao, A. N. Jaynes, S. Kanekal, X. Li, S. Elkington, Multiyear measurements of radiation belt electrons: Acceleration, transport, and loss. *J. Geophys. Res. Space Physics* **124**, 2588–2602 (2019).
3. Y. Y. Shprits, D. Subbotin, A. Drozdov, M. E. Usanova, A. Kellerman, K. Orlova, D. N. Baker, D. L. Turner, K.-C. Kim, Unusual stable trapping of the ultrarelativistic electrons in the Van Allen radiation belts. *Nat. Phys.* **9**, 699–703 (2013).
4. R. M. Millan, D. N. Baker, Acceleration of particles to high energies in earth's radiation belts. *Space Sci. Rev.* **173**, 103–131 (2012).
5. R. B. Horne, R. M. Thorne, Potential waves for relativistic electron scattering and stochastic acceleration during magnetic storms. *Geophys. Res. Lett.* **25**, 3011–3014 (1998).
6. A. Y. Ukhorskiy, M. I. Sitnov, Dynamics of radiation belt paticles. *Space Sci. Rev.* **179**, 545–578 (2013).
7. R. B. Horne, R. M. Thorne, Y. Y. Shprits, N. P. Meredith, S. A. Glauert, A. J. Smith, S. G. Kanekal, D. N. Baker, M. J. Engebretson, J. L. Posch, M. Spasojevic, U. S. Inan, J. S. Pickett, P. M. E. Decreau, Wave acceleration of electrons in the Van Allen radiation belts. *Nature* **437**, 227–230 (2005).
8. E. E. Woodfield, R. B. Horne, S. A. Glauert, J. D. Menietti, Y. Y. Shprits, The origin of Jupiter's outer radiation belt. *J. Geophys. Res. Space Physics* **119**, 3490–3502 (2014).
9. R. B. Horne, T. Kersten, S. A. Glauert, N. P. Meredith, D. Boscher, A. Sicard-Piet, R. M. Thorne, W. Li, A new diffusion matrix for whistler mode chorus waves. *J. Geophys. Res. Space Physics* **118**, 6302–6318 (2013).
10. J. C. Ingraham, T. E. Cayton, R. D. Belian, R. A. Christensen, R. H. W. Friedel, M. M. Meier, G. D. Reeves, M. Tuszewski, Substorm injection of relativistic electrons to geosynchronous orbit during the great magnetic storm of March 24, 1991. *J. Geophys. Res. Space Physics* **106**, 25759–25776 (2001).
11. C. Katsavrias, I. Sandberg, W. Li, O. Podladchikova, I. A. Daglis, C. Papadimitriou, C. Tsironis, S. Aminalragia-Giamini, Highly relativistic electron flux enhancement during the weak geomagnetic storm of April–May 2017. *J. Geophys. Res. Space Physics* **124**, 4402–4413 (2019).
12. H. J. Allison, Y. Y. Shprits, Local heating of radiation belt electrons to ultra-relativistic energies. *Nat. Commun.* **11**, 4533 (2020).
13. B. W. Sheeley, M. B. Moldwin, H. K. Rassoul, R. R. Anderson, An empirical plasmasphere and trough density model: CRRES observations. *J. Geophys. Res. Space Physics* **106**, 25631–25641 (2001).
14. R. E. Denton, J. D. Menietti, J. Goldstein, S. L. Young, R. R. Anderson, Electron density in the magnetosphere. *J. Geophys. Res. Space Physics* **109**, A09215 (2004).
15. D. L. Carpenter, R. R. Anderson, An ISEE/whistler model of equatorial electron density in the magnetosphere. *J. Geophys. Res. Space Physics* **97**, 1097–1108 (1992).
16. C. A. Kletzing, W. S. Kurth, M. Acuna, R. J. MacDowall, R. B. Torbert, T. Averkamp, D. Bodet, S. R. Bounds, M. Chutter, J. Connerney, D. Crawford, J. S. Dolan, R. Dvorsky, G. B. Hospodarsky, J. Howard, V. Jordanova, R. A. Johnson, D. L. Kirchner, B. Mokrzycki, G. Needell, J. Odom, D. Mark, R. Pfaff Jr., J. R. Phillips, C. W. Piker, S. L. Remington, D. Rowland, O. Santolik, R. Schnurr, D. Sheppard, C. W. Smith, R. M. Thorne, J. Tyle, The Electric and Magnetic Field Instrument Suite and Integrated Science (EMFISIS) on RBSP. *Space Sci. Rev.* **179**, 127–181 (2013).
17. I. S. Zhelavskaya, M. Spasojevic, Y. Y. Shprits, W. S. Kurth, Automated determination of electron density from electric field measurements on the Van Allen probes spacecraft. *J. Geophys. Res. Space Physics* **121**, 4611–4625 (2016).
18. M. Spasojevic, Y. Y. Shprits, Chorus functional dependencies derived from CRRES data. *Geophys. Res. Lett.* **40**, 3793–3797 (2013).
19. D. Wang, Y. Y. Shprits, I. S. Zhelavskaya, O. V. Agapitov, A. Y. Drozdov, N. A. Aseev, Analytical chorus wave model derived from Van Allen Probe observations. *J. Geophys. Res. Space Physics* **124**, 1063–1084 (2019).
20. X. Tao, F. Zonca, L. Chen, Y. Wu, Theoretical and numerical studies of chorus waves: A review. *Sci. China Earth Sci.* **63**, 78–92 (2019).
21. R. B. Horne, S. A. Glauert, R. M. Thorne, Resonant diffusion of radiation belt electrons by whistler-mode chorus. *Geophys. Res. Lett.* **30**, 1493 (2003).
22. J. M. Albert, Diffusion by one wave and by many waves. *J. Geophys. Res. Space Physics* **115**, A00F05 (2010).
23. J. M. Albert, Gyroresonant interactions of radiation belt particles with a monochromatic electromagnetic wave. *J. Geophys. Res.* **105**, 21191–21209 (2000).
24. X.-J. Zhang, O. Agapitov, A. V. Artemyev, D. Mourenas, V. Angelopoulos, W. S. Kurth, J. W. Bonnell, G. B. Hospodarsky, Phase decoherence within intense chorus wave packets constrains the efficiency of nonlinear resonant electron acceleration. *Geophys. Res. Lett.* **47**, e2020GL089807 (2020).
25. W. E. Drummond, D. Pines, Nonlinear plasma oscillations. *Ann. Phys. Rehabil. Med.* **28**, 478–499 (1964).
26. C. F. Kennel, F. Engelmann, Velocity space diffusion from weak plasma turbulence in a magnetic field. *Phys. Fluids* **9**, 2377–2388 (1966).
27. I. Lerche, Quasilinear theory of resonant diffusion in a magneto-active, relativistic plasma. *Phys. Fluids* **11**, 1720–1727 (1968).
28. Y. Y. Shprits, D. A. Subbotin, N. P. Meredith, S. R. Elkington, Review of modeling of losses and sources of relativistic electrons in the outer radiation belt II: Local acceleration and loss. *J. Atmos. Sol. Terr. Phys.* **70**, 1694–1713 (2008).
29. C.-G. Fälthammar, Effects of time-dependent electric fields on geomagnetically trapped radiation. *J. Geophys. Res.* **70**, 2503–2516 (1965).
30. H. J. Allison, R. B. Horne, S. A. Glauert, G. Del Zanna, On the importance of gradients in the low-energy electron phase space density for relativistic electron acceleration. *J. Geophys. Res. Space Physics* **124**, 2628–2642 (2019).
31. Y. Y. Shprits, R. M. Thorne, R. B. Horne, S. A. Glauert, M. Cartwright, C. T. Russell, D. N. Baker, S. G. Kanekal, Acceleration mechanism responsible for the formation of the new radiation belt during the 2003 Halloween solar storm. *Geophys. Res. Lett.* **33**, L05104 (2006).
32. R. M. Thorne, W. Li, B. Ni, Q. Ma, J. Bortnik, L. Chen, D. N. Baker, H. E. Spence, G. D. Reeves, M. G. Henderson, C. A. Kletzing, W. S. Kurth, G. B. Hospodarsky, J. B. Blake, J. F. Fennell, S. G. Claudepierre, S. G. Kanekal, Rapid local acceleration of relativistic radiation-belt electrons by magnetospheric chorus. *Nature* **504**, 411–414 (2013).
33. S. J. Bame, J. R. Asbridge, H. E. Felthauser, E. W. Hones, I. B. Strong, Characteristics of the plasma sheet in the Earth's magnetotail. *J. Geophys. Res.* **72**, 113–129 (1967).
34. D. Wang, Y. Y. Shprits, On how high-latitude chorus waves tip the balance between acceleration and loss of relativistic electrons. *Geophys. Res. Lett.* **46**, 7945–7954 (2019).
35. F. Xiao, Z. Su, H. Zheng, S. Wang, Three-dimensional simulations of outer radiation belt electron dynamics including cross-diffusion terms. *J. Geophys. Res. Space Physics* **115**, A05216 (2010).
36. Z. Su, F. Xiao, H. Zheng, Z. He, H. Zhu, M. Zhang, C. Shen, Y. Wang, S. Wang, C. A. Kletzing, W. S. Kurth, G. B. Hospodarsky, H. E. Spence, G. D. Reeves, H. O. Funsten, J. B. Blake, D. N. Baker, Nonstorm time dynamics of electron radiation belts observed by the Van Allen probes. *Geophys. Res. Lett.* **41**, 229–235 (2014).
37. Y. Y. Shprits, R. B. Horne, A. C. Kellerman, A. Y. Drozdov, The dynamics of Van Allen belts revisited. *Nat. Phys.* **14**, 102–103 (2018).
38. Y. Y. Shprits, B. Ni, Dependence of the quasi-linear scattering rates on the wave normal distribution of chorus waves. *J. Geophys. Res. Space Physics* **114**, A11205 (2009).
39. B. Ni, Resonant scattering of plasma sheet electrons by whistler-mode chorus: Contribution to diffuse auroral precipitation. *Geophys. Res. Lett.* **35**, L11106 (2008).
40. K. G. Orlova, Y. Y. Shprits, On the bounce-averaging of scattering rates and the calculation of bounce period. *Phys. Plasmas* **18**, 092904 (2011).
41. D. Subbotin, Y. Shprits, B. Ni, Three-dimensional VERB radiation belt simulations including mixed diffusion. *J. Geophys. Res. Space Physics* **115**, A03205 (2010).
42. B. Ni, R. M. Thorne, N. P. Meredith, R. B. Horne, Y. Y. Shprits, Resonant scattering of plasma sheet electrons leading to diffuse auroral precipitation: 2. Evaluation for whistler mode chorus waves. *J. Geophys. Res. Space Physics* **116**, A04219 (2011).
43. H. Zhu, Y. Y. Shprits, M. Spasojevic, A. Y. Drozdov, New hiss and chorus waves diffusion coefficient parameterizations from the Van Allen probes and their effect on long-term

relativistic electron radiation-belt VERB simulations. *J. Atmos. Sol. Terr. Phys.* **193**, 105090 (2019).
44. N. A. Tsyganenko, M. I. Sitnov, Modeling the dynamics of the inner magnetosphere during strong geomagnetic storms. *J. Geophys. Res. Space Physics* **110**, A03208 (2005).
45. I. Zhelavskaya, Y. Shprits, M. Spasojevic, W. Kurth, A. Y. Ukhorskiy, M. I. Sitnov, Electron density derived with the Neural-network-based Upper-hybrid Resonance Determination algorithm from the Van Allen Probes EMFISIS measurements, (2020), Data product; http://doi.org/10.5880/GFZ.2.8.2020.002.

Acknowledgments: We thank A. Drozdov, R. Horne, S. Glauert, N. Meredith, O. Allanson, and M. Clilverd for the useful discussions regarding the work presented here. Y.Y.S. would also like to acknowledge helpful discussions with R. M. Thorne. We acknowledge the NASA Van Allen Probe team and H. E. Spence and C. Kletzing for use of the REPT and EMFISIS data. **Funding:** This work was funded by NASA H-SR funding NNX15AI94G, NSF GEM AGS-1203747, Helmholtz-Gemeinshaft (HGF), Deutsche Forschungsgemeinschaft (DFG) through grant CRC 1294 "Data Assimilation"–Project B06, and machine learning based plasma density model (MAP) pilot project funded by the Helmholtz Association ZT-I-0022. H.J.A. received funding from the Alexander von Humboldt Foundation. I.S.Z. was supported by Geo.X, the Research Network for Geosciences in Berlin and Potsdam, under grant no. SO_087_GeoX. Y.Y.S. acknowledges funding from the European Union's Horizon 2020 research and innovation program under grant agreement no. 870452 (PAGER). **Author contributions:** Y.Y.S. and H.J.A. conceived and designed the study. H.J.A. performed the analysis with contribution from A.G.S. H.J.A. performed the model runs. I.S.Z. provided the electron density data. D.W. processed the chorus wave data for the October 2015 example. H.J.A., Y.Y.S., and D.W. interpreted the results. H.J.A. wrote the manuscript with input from all coauthors. **Competing interests:** The authors declare that they have no competing interests. **Data and materials availability:** All data needed to evaluate the conclusions in the paper are present in the paper and/or the Supplementary Materials. The electron density dataset was derived from EMFISIS data using the NURD algorithm and is available at the GFZ Data Services (*45*), as well as from ftp://ftp.gfz-potsdam.de/home/rbm/NURD/. Van Allen Probe EMFISIS data can be accessed through the EMFISIS website, http://emfisis.physics.uiowa.edu/data/index, and the REPT data from https://rbsp-ect.newmexicoconsortium.org/data_pub/. All geomagnetic indices used in the study were downloaded from the SPDF OMNIWeb. Additional data related to this paper may be requested from the authors.

Submitted 3 April 2020
Accepted 11 December 2020
Published 29 January 2021
10.1126/sciadv.abc0380

Citation: H. J. Allison, Y. Y. Shprits, I. S. Zhelavskaya, D. Wang, A. G. Smirnov, Gyroresonant wave-particle interactions with chorus waves during extreme depletions of plasma density in the Van Allen radiation belts. *Sci. Adv.* **7**, eabc0380 (2021).

Science Advances

Gyroresonant wave-particle interactions with chorus waves during extreme depletions of plasma density in the Van Allen radiation belts

Hayley J. Allison, Yuri Y. Shprits, Irina S. Zhelavskaya, Dedong Wang and Artem G. Smirnov

Sci Adv **7** (5), eabc0380.
DOI: 10.1126/sciadv.abc0380